ENVIRONMENTAL SCIENCES

A tale of two coasts: Unveiling US Gulf and Atlantic coastal cities at high flood risk

Hemal Dey[1,2] and Wanyun Shao[1,2,3]*

Coastal flooding is increasing, with accelerating impacts ahead. Its impact, however, can be mitigated through proactive risk management, requiring comprehensive risk assessment. Using the US Gulf and Atlantic Coasts (USGAC) as a test bed, this study develops a framework to identify high-risk coastal cities and reveal underlying factors under dual-risk scenarios—general flood damage (GFD) and extreme flood damage (EFD). Using historical flood damage data and 16 factors representing hazard, exposure, and vulnerability, this study adopts three machine learning models—support vector machine, random forest, and multilayer perceptron—to assess flood risk. This study identifies eight coastal cities at high flood risk where New York City has the largest population at risk (GFD: 4.75 million; EFD: 4.40 million) and New Orleans City has the highest relative exposure (~99% under both). Coastal flood risk is greatest in low-lying, densely developed urban areas with high drainage density. Overall, this scalable framework offers actionable insights for policy-makers to manage floods in other flood-prone regions.

INTRODUCTION

Floods cause substantial losses of lives and damage to infrastructure worldwide. According to the Emergency Events Database (EM-DAT), between 1900 and 2021, flooding caused 7 million deaths, affected 38 million people, and resulted in $1.3 trillion in economic losses (*1*). The increasing frequency and severity of flood events are leading to an increasing number of people at high risk. Worldwide, ~1.81 billion people (23% of the global population) are directly exposed to 100-year floods (flood level with 1% annual probability of exceedance). About $9.8 trillion in economic activities (12% of the global gross domestic product in 2020) is directly located in substantial flood risk areas (*2*).

In the US, flooding is the costliest natural disaster causing billions of dollars in annual losses in property damages and agricultural losses (*3*). The US has the second-highest economic values at risk from floods, with $1.1 trillion in potential assets exposed (*2*). Researchers project that by, 2050, sea levels along US coastlines will rise by 0.25 to 0.3 m, increasing the risk of severe flooding in major coastal cities (*4*). Along the US Gulf and Atlantic Coasts (USGAC) (Fig. 1), hurricane-induced flood risks are increasing due to sea level rise, threatening the coastal population and infrastructure (*5*). Now, about 30% of counties along the USGAC are at high flood risk, with low resilience and high social vulnerability and the risk is projected to be elevated in the future (*6*).

It is thus imperative for coastal communities along the USGAC to adopt effective risk mitigation to build societal resilience to flooding. Integrated flood risk assessment supports proactive risk management as it provides an empirical foundation that is needed to understand where risks are concentrated and why they emerge. Flood risk modeling plays a critical role in effective risk mitigation as it helps identify vulnerable communities and underlying causative risk factors and assess potential damages (*7*, *8*). The increasing flood risk highlights the urgent need to develop a comprehensive flood risk assessment framework. Considering the complexity of flooding impacts, both physical and social dimensions of factors must be incorporated in this comprehensive risk assessment framework (*9*). This study presents such a comprehensive framework for flood risk assessment that integrates hazard, exposure, and vulnerability.

To effectively assess flood risk, it is essential to first establish clear definitions. Flood risk refers to the likelihood of a flood event occurring with the potential adverse impacts on society and the environment (*10*–*12*). It is thus determined by the interplay of three interconnected components: hazard, exposure, and vulnerability (*13*). Hazard refers to the probability of flood occurrence, influenced by the natural characteristics of a region (*14*). Exposure refers to the presence of populations, their infrastructures and resources that are exposed to potential flooding (*15*). Vulnerability refers to the preexisting socioeconomic condition that hinders a community from effectively mitigating the adverse impacts of a disaster (*6*). Combining all of them can thus provide more precise estimation of flood risk (*15*).

The recent advancements in geographic information systems, remote sensing, and cloud computing offer a powerful platform for integrating and analyzing geospatial data for flood assessment (*1*). Various methods have been developed using these technologies. These methods include bivariate statistical models [e.g., frequency ratio (FR)], multicriteria decision-making models [e.g., analytic hierarchy process (AHP)], physics-based models [e.g., Hydrologic Engineering Center–River Analysis System (HECRAS)], and machine learning (ML) models [e.g., random forest (RF)] (*7*, *16*). Each method has its own distinct advantages and limitations. Specifically, the FR tends to oversimplify the relationship between flood and its causative factors, which could cause substantial estimation errors (*17*); the AHP needs experts' opinions, introducing biases into the assessment (*18*); the HECRAS model requires large data, substantial computational resources, and, involves parameters that take a long time to prepare (*16*). Despite some limitations such as high data dependency and a lack of interpretability, ML models have played an increasingly important role in flood risk assessment by offering better performance, cost-effective solutions, and flexible and faster processing compared to conventional approaches (*7*, *19*). They can effectively capture nonlinear relationships and complex interactions between flood occurrence and flood contributing factors without requiring expert opinions or incurring high computational cost (*17*, *20*). In addition, explainable artificial intelligence (XAI) techniques, such as the Shapley additive explanations (SHAP) model, can help interpret these ML predictions by analyzing the

[1]Department of Geography & the Environment, The University of Alabama, Tuscaloosa, AL, USA. [2]Alabama Water Institute, The University of Alabama, Tuscaloosa, AL, USA. [3]Institute for Social Science Research, The University of Alabama, Tuscaloosa, AL, USA. *Corresponding author. Email: wshao1@ua.edu

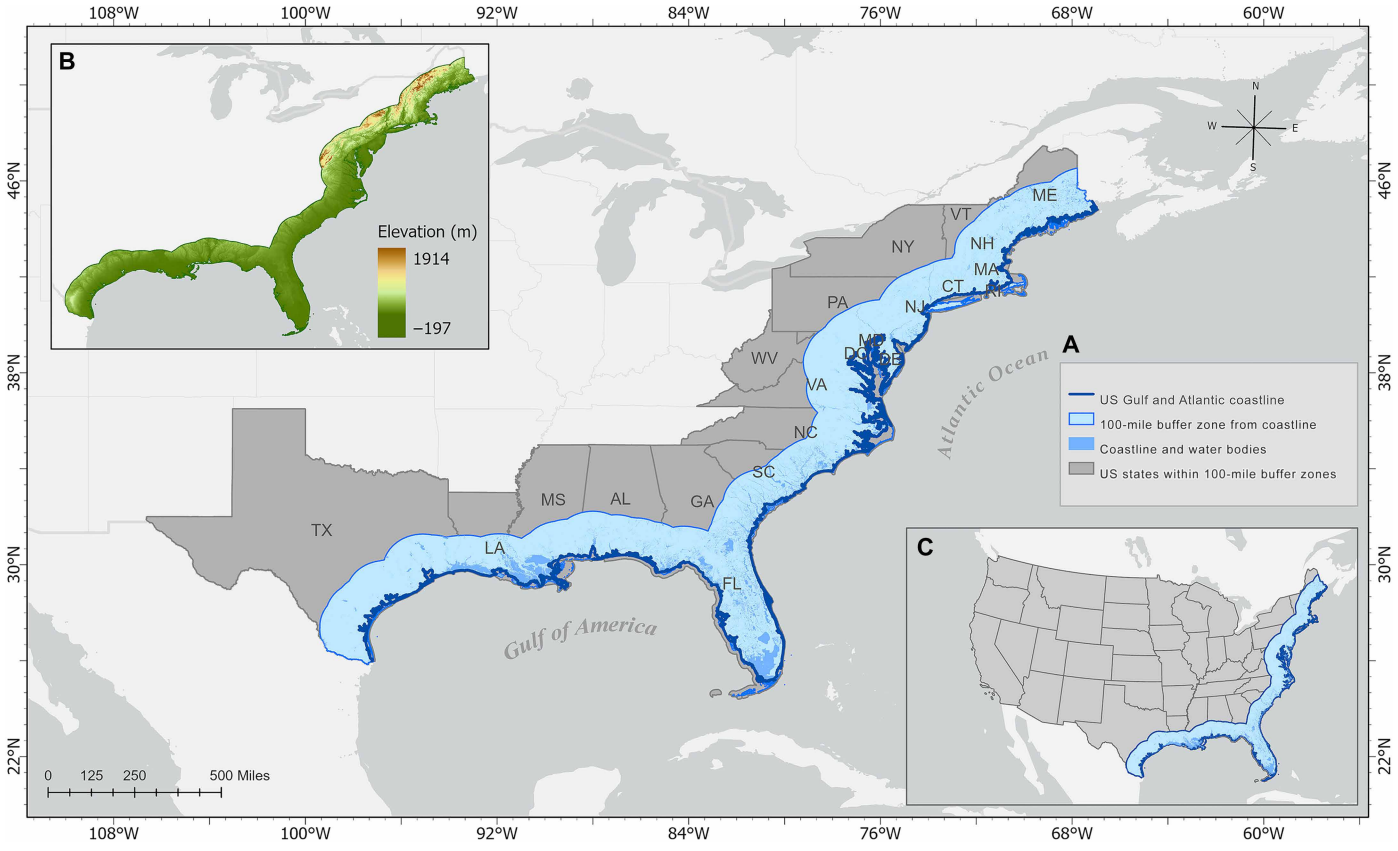

Fig. 1. Study area map. (**A**) 100-mile buffer zones from the US Gulf and Atlantic coastlines. (**B**) Elevation map of the USGAC. (**C**) Location of the USGAC in the context of the CONUS.

contribution of factors and identifying the most influential drivers on flood risk (*21*). Thus, they have gained widespread popularity in flood risk assessment in the past two decades.

To date, numerous ML models have been used to predict flood hazards, including linear models such as logistic regression (*22*) and support vector machine (SVM) (*23*); ensemble tree–based models such as decision tree (*24*), RF (*17*), XGBoost (*14*), and LightGBM (*12*); and neural network models including artificial neural network (ANN) (*25*) and convolutional neural network (CNN) (*26*). Correspondingly, this study uses three widely popular ML models—SVM, RF, and multilayer perceptron (MLP)—representing the linear, tree-based, and neural network algorithm families, respectively, to evaluate and compare their predictive accuracies (Fig. 2).

The predictive accuracy of ML models in flood risk modeling largely depends on the training process. Although researchers commonly use historical flood inundation data as the target variable and relevant flood risk factors (FRFs) as predictors to train the models, flood inundation data that are solely derived from Sentinel-1 SAR can lead to inaccuracies in predictions due to several limitations, including the absence of peak flood-time imagery, speckle noise, unclear water boundaries, and interference from vegetation and urban areas (*27*). Many recent studies (*6*, *20*, *28*) strongly advocate for incorporating historical flood damage data along with their precise damage locations and level of severities to train ML models. Moreover, many recent studies emphasize that a comprehensive flood risk assessment should integrate a wider range of factors beyond hydrologic hazard data (*29*, *30*). Incorporating factors representing both exposure and vulnerability alongside hazard data can build more accurate and operational flood risk models (*3*, *6*, *20*).

Despite increasing awareness, few studies have integrated precise historical flood damage data with a comprehensive set of risk factors encompassing hazard, exposure, and vulnerability in flood risk modeling. Although previous research on the US coastal flood risk has made important contributions, several key gaps remain to be addressed. The National Risk Index (NRI) applied k-means clustering, an unsupervised clustering algorithm, analyzing data at the census tract level across the contiguous US (CONUS) but heavily relied on aggregated indices with notable methodological limitations (*31*). Ohenhen *et al.* (*4*) estimated potential flood inundation across 32 major US coastal cities by integrating vertical land motion and elevation datasets with sea level rise projections yet excluded critical risk factors, especially exposure and vulnerability. Sajjad *et al.* (*6*) assessed flood risk at the county level under current and future scenarios, yet their framework was restricted to hazards, vulnerability, and resilience, excluding exposure. Yarveysi *et al.* (*31*) analyzed flood risk at the census block group level along the Gulf Coast but only included precipitation probability and storm surge height to represent hazard, which fails to consider a full range of nonlinear interactions among multiple hazard drivers. There is thus an urgent need for a comprehensive flood risk assessment framework that (i) incorporates observed flood damage data rather than proxies; (ii) distinguishes between general and extreme flood risks at fine spatial scales; (iii) includes a wide range of FRFs, fully

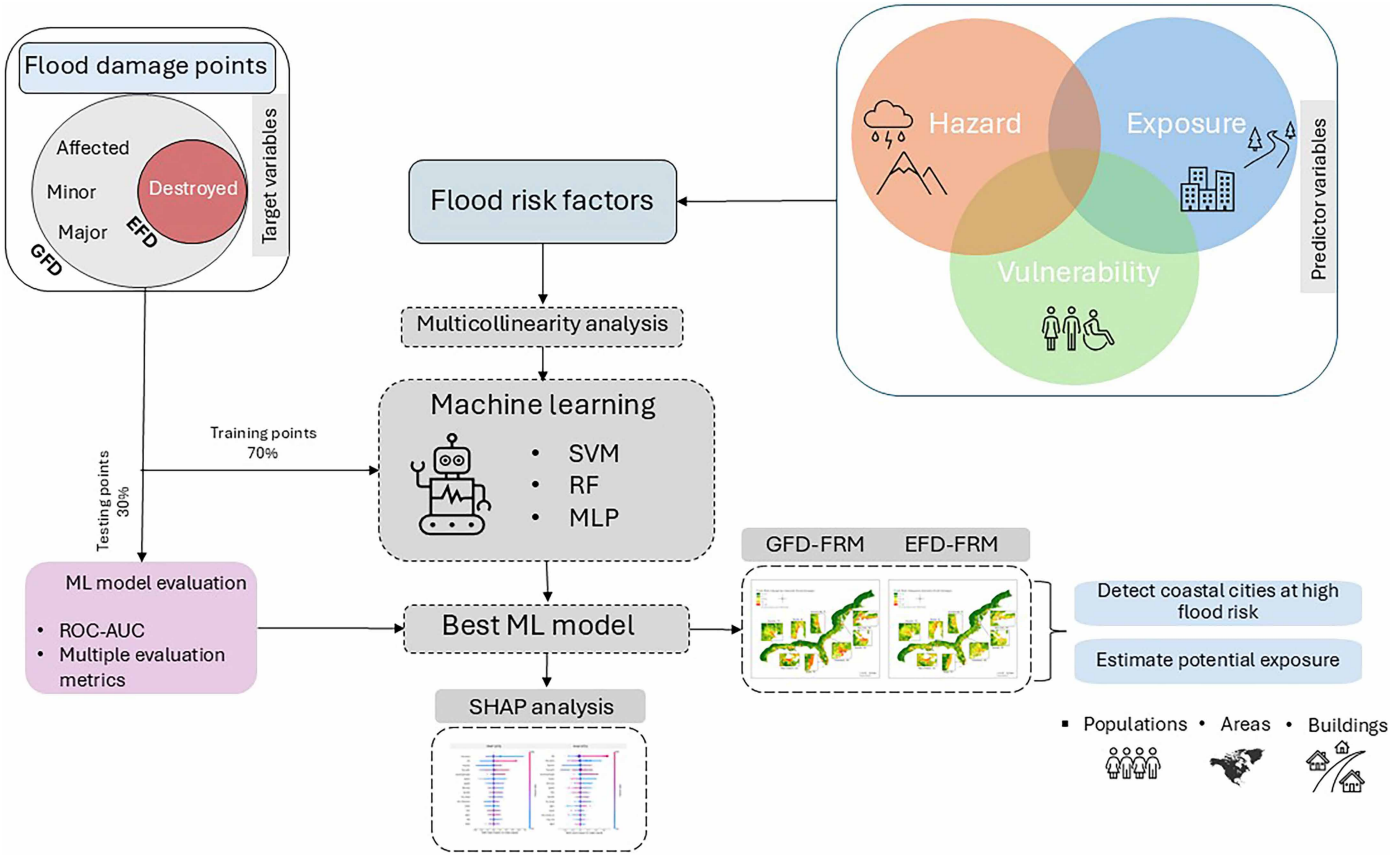

Fig. 2. Conceptual framework.

capturing the interactions among hazards, exposure, and vulnerability; and (iv) identifies the key drivers of risk among at-risk USGAC cities while providing specific policy recommendations.

In particular, the present study develops a robust and comprehensive dual-scenario framework that uses precise flood damage data as target variables under two scenarios: general flood damage (GFD; property damage at all severity levels) and extreme flood damage (EFD; fully destroyed properties only) and a comprehensive set of FRFs (Fig. 2). By distinguishing between these two outcomes, the framework reveals more nuanced spatial patterns and underlying drivers of flood risk. In particular, this study unveils top at-risk cities along the USGAC by estimating potential exposure under GFD and EFD scenarios, complemented by a comparative analysis of top two at-risk cities with policy recommendations for long-term risk mitigation.

This framework combines advanced ML techniques with multidimensional data to provide more accurate flood risk predictions, which is scalable and replicable to other regions prone to flooding. The resulting flood risk map, produced by this framework, can serve as a data-driven foundation for informed decision-making, enabling policymakers to prioritize interventions, allocate resources efficiently, and design targeted adaptation and mitigation strategies for future flood scenarios under different levels of potential damage. By facilitating improved flood management, this framework contributes to strengthening community resilience worldwide. In addition, the policy guidance offered through this study supports the development of resilient coastal communities capable of effectively responding to flood hazards.

RESULTS

ML model's accuracy test

The receiver operating characteristic area under the curve (ROC-AUC) reveals that all ML models achieve high performances under both flood damage scenarios, where RF and MLP have a score of 0.99 and an SVM score of 0.97 (Fig. 3, A and B). Because RF and MLP have identical ROC-AUC scores, the study further evaluates these ML models using additional metrics including accuracy, precision, recall, F1 score, kappa score, and Jaccard score. On the basis of the average of these metrics score, RF performs the best, with an average score of 0.95 under the GFD scenario and 0.96 under the EFD scenario, followed by MLP with the mean scores of 0.93 under GFD and 0.94 under EFD whereas with an SVM score of 0.89 in both cases (Fig. 3, C and D). Therefore, this study adopts the RF model for further analysis.

Flood risk maps of the USGAC under GFD and EFD

The analysis reveals a concerning trend in the distribution of flood risk zones along the USGAC. Although a small portion of the area within a buffer zone of 100 miles (≈160.934 km) of the USGAC falls under high or very high flood risk, a substantial number of population is concentrated in the high-risk area. Under the GFD scenario, 1.1% of the area (10,083.75 km^2) is classified as at very high risk with 16.7% of the population (17.52 million people). A total of 3.5% of the area (30,798.51 km^2) is classified as at high risk, where 16.21% of the population (17.02 million) live. A total of 8.6% of the area (76,217.75 km^2) and 20.4% of the population (21.47 million) are

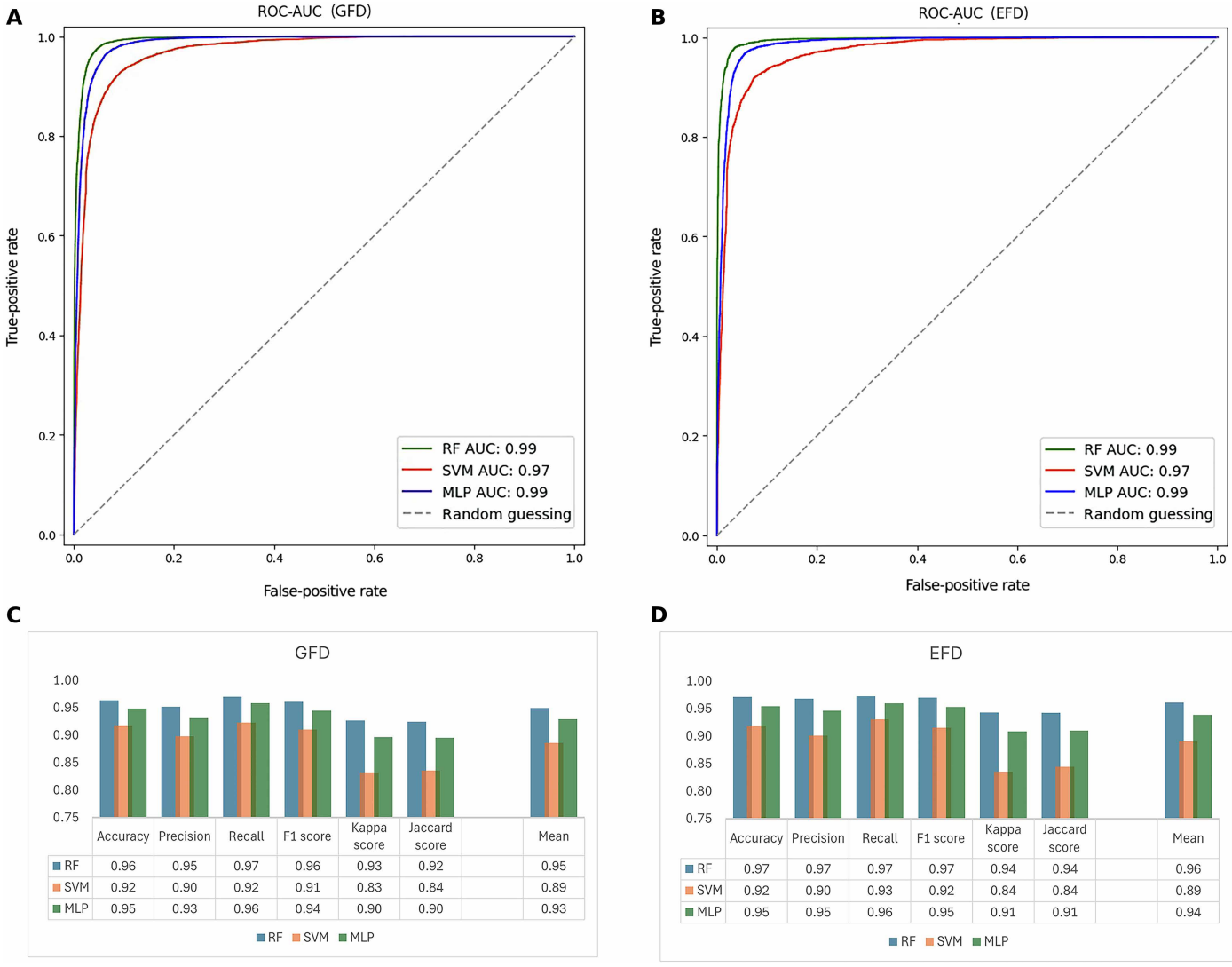

Fig. 3. Performance evaluation of ML models under different flood damage scenarios. (**A**) ROC-AUC under the GFD scenario. (**B**) ROC-AUC under the EFD scenario. (**C**) Multiple evaluation metrics under the GFD scenario. (**D**) Multiple evaluation metrics under the EFD scenario.

classified as at moderate risk (Fig. 4A). Under the more severe EFD scenario (Fig. 4B), only 0.5% of the area (4,678.88 km^2) is at very high risk, yet 4.1% of the population (4.29 million) lives there. High-risk zones expand to 3.9% of the area (34,621.13 km^2), with 19.5% of the population (20.49 million). Moderate risk areas cover 13.6% of the area (120,120.62 km^2), with 31.1% of the population (32.66 million).

Coastal cities that are at high flood risk

The analysis further identifies eight coastal cities, namely, New York, NY; Norfolk, VA; Charleston, SC; Jacksonville, FL; Miami, FL; Mobile, AL; New Orleans, LA; and Houston, TX, that are at very high or high flood risk. Table 1 demonstrates the percentage of area, total exposed population, the percentage of exposed population, the number of exposed buildings, and the percentage of exposed buildings under both the GFD and EFD scenarios for these eight cities.

In terms of total exposed population, New York, NY ranks first under both scenarios, with ~4.75 million people exposed under GFD and 4.40 million under EFD. Houston, TX is second, with 0.6 million exposed under GFD and 1.35 million under EFD. Jacksonville, FL is third, with 0.68 million exposed under GFD and 0.43 million under EFD [Fig. 4D(i)]. By percentage of exposed population within each city, New Orleans, LA ranks first, with 98.97% under the GFD scenario and 98.11% under EFD. Miami, FL is second, with 84.60% of its population exposed under GFD and 57.78% under EFD. Norfolk, VA is third, with 83.45% exposed under GFD and 56.94% under EFD [Fig. 4D(ii)].

In terms of total exposed human infrastructures, New York, NY has the highest number of buildings at high flood risk, with ~0.23 million in the GFD scenario and 0.21 million in the EFD scenario. The second-highest is Jacksonville, FL with 0.21 million buildings in the GFD scenario, whereas Houston, TX ranks second in the EFD scenario with 0.2 million buildings (Table 1). In terms of the percentage of exposed human infrastructure, New Orleans, LA has the highest proportion of buildings at high flood risk, with 99.52% in the GFD scenario and 99.35% in the EFD scenario (Table 1). Miami, FL ranks second, with 96.42% under GFD and 65.86% under EFD.

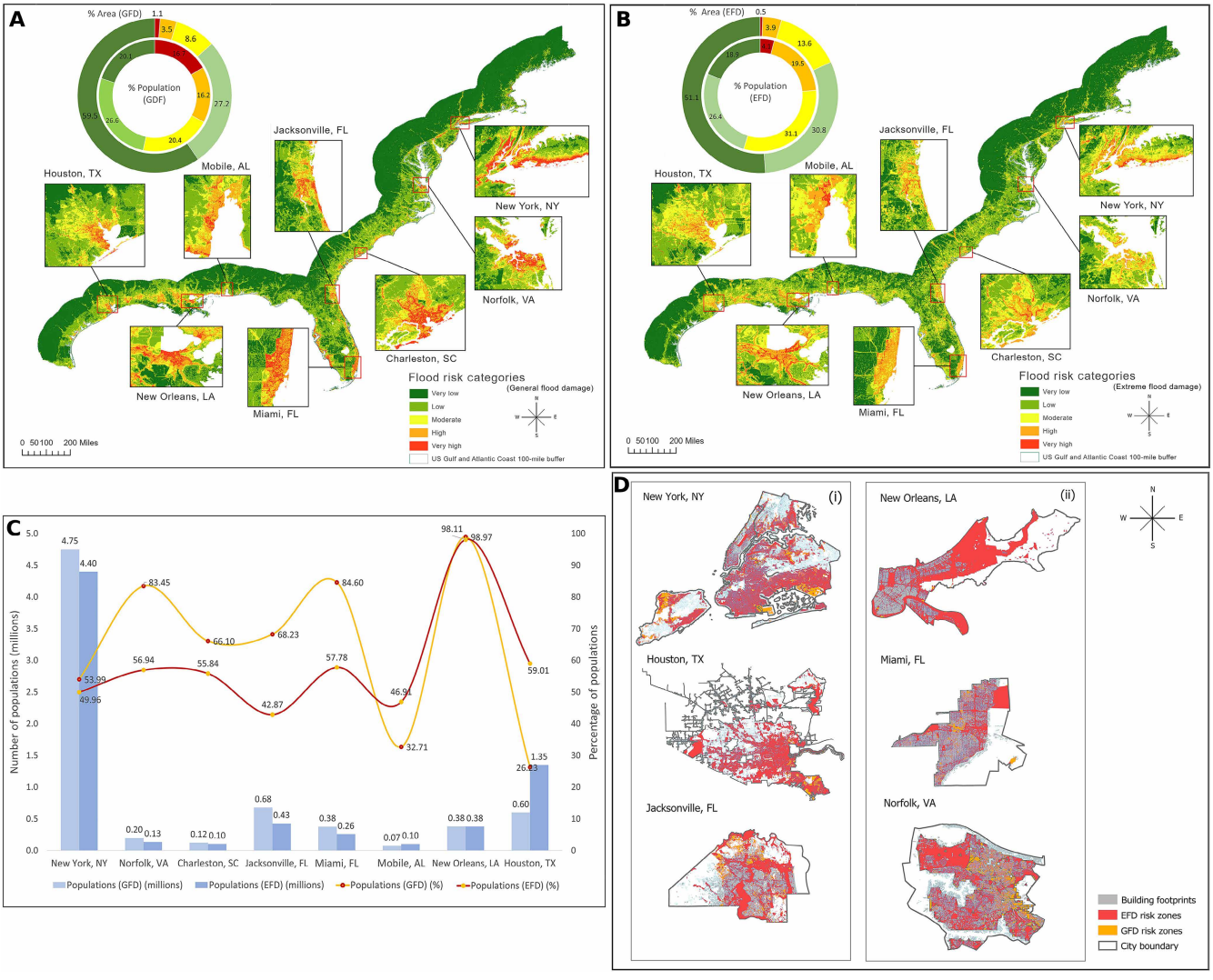

Fig. 4. Flood risk distribution along the USGAC. (**A**) Flood risk map (FRM) under the GFD scenario. (**B**) FRM under the EFD scenario. (**C**) Combined bar chart of the total and percentage of exposed population in at-risk cities across the USGAC. (**D**) Top cities where substantial population and infrastructure are exposed to very high and high flood risk: (i) top three cities in terms of total exposed population and (ii) top three cities in terms of percentages of exposed population.

Underlying factor analysis

The SHAP analysis reveals that elevation, drainage density, population density, precipitation, building height, and distance from river or coast are the top six underlying factors for both GFD and EFD scenarios.

Under the GFD scenario, low elevation emerges as the primary factor increasing flood risk, followed by high drainage density and high population density (Fig. 5A), because low-lying areas are inherently more susceptible to any level of flooding, reinforcing the foundational role played by topography in determining flood risk. On the other hand, under the EFD scenario, high drainage density is the primary contributor followed by low elevation and high population density (Fig. 5B). Drainage density is defined as the total length of streams and rivers per unit of watershed areas. High drainage density means that water encounters a channel quickly after rainfall, resulting in shortening water travel time, accelerating runoff concentration, and rapid rises in streamflow. Watersheds with high drainage density are often observed to have impermeable soil, shallow bedrock, steep slopes, and extensive impervious surfaces. The regions characterized by extensive and complex drainage networks are more prone to catastrophic flooding, although drainage density itself is not inherently detrimental. Rather, human interventions and overburdened man-made infrastructure within high-drainage regions amplify the potential risk for EFD as they fundamentally alter the landscape that determines how quickly and efficiently rainfall is converted into surface runoff and delivered to stream channels. Population density consistently ranks the third most powerful factor in both scenarios, indicating that concentrated human settlements can increase societal exposure to flood damage, regardless of event severity.

DISCUSSION

This study presents a robust and comprehensive framework for flood risk modeling by integrating historical flood damage data with a comprehensive set of FRFs under dual scenarios—GFD and EFD—using

Table 1. Estimated areas, populations, and buildings at very high and high flood risk in the most at-risk cities along the USGAC.

Vulnerable cities	GFD-FRM					EFD-FRM				
	Areas (%)	Populations	Populations (%)	Buildings	Buildings (%)	Areas (%)	Populations	Populations (%)	Buildings	Building (%)
New York, NY	54.2	4,752,243	53.99	232,269	50.85	45.75	4,396,867	49.96	215,956	47.28
Norfolk, VA	88.13	197,200	83.45	54,165	80.77	63.45	134,552	56.94	32,948	49.13
Charleston, SC	67.08	123,328	66.10	39,978	83.89	39.76	104,179	55.84	17,973	37.71
Jacksonville, FL	47.73	679,251	68.23	219,494	70.20	36.65	426,846	42.87	130,677	41.79
Miami, FL	90.01	376,311	84.60	58,735	96.46	72.92	257,020	57.78	40,105	65.86
Mobile, AL	38.94	71,357	32.71	32,696	40.74	55.36	102,342	46.91	41,990	52.32
New Orleans, LA	52.5	380,057	98.97	128,962	99.52	69.1	376,751	98.11	128,758	99.35
Houston, TX	26.35	599,371	26.23	108,629	26.84	48.47	1,348,627	59.01	207,034	51.15

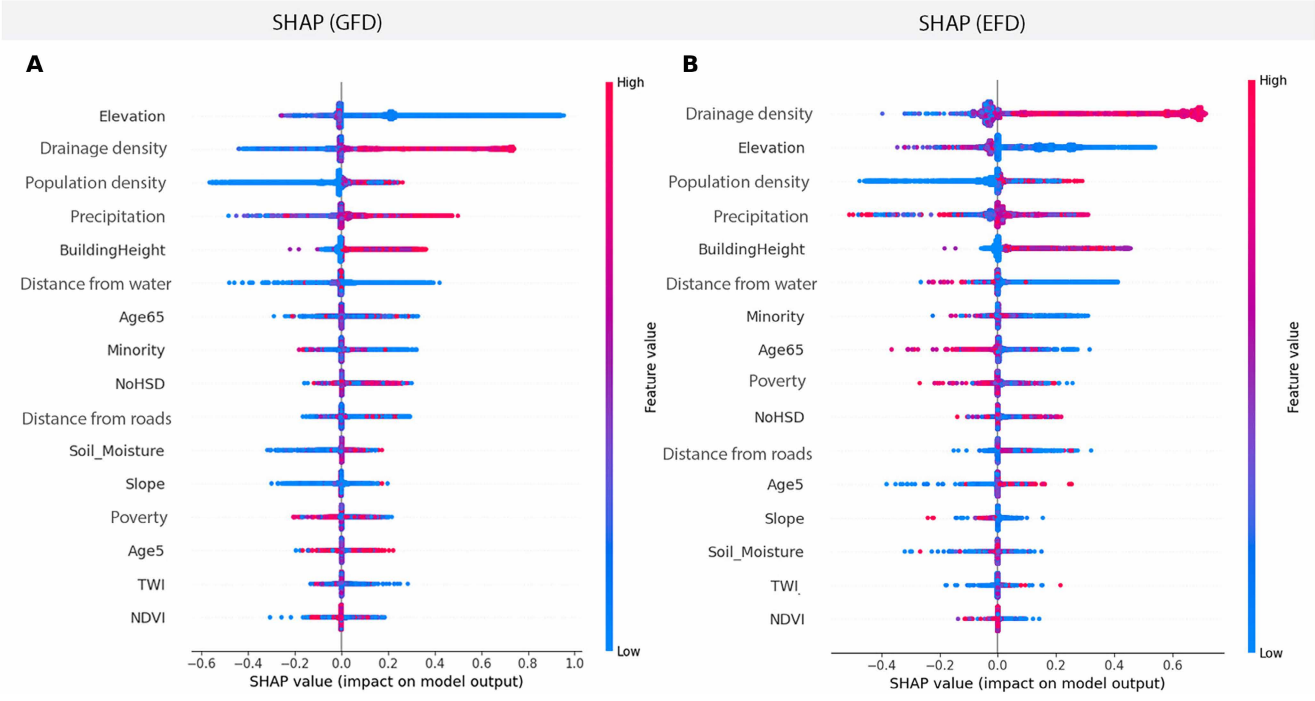

Fig. 5. SHAP analysis. (**A**) Ranks of underlying FRFs for GFD. (**B**) Ranks of underlying FRFs for EFD. The *x* axis represents SHAP values, where positive values indicate a higher contribution to flood risk and negative values indicate a lower contribution. The primary *y* axis lists the FRFs, whereas the secondary *y* axis shows the corresponding value ranges of these FRFs. Red points represent higher FRF values, whereas blue points represent lower values.

geospatial artificial intelligence (GeoAI) techniques. This approach unveils top flood-risk cities along the USGAC and reveals the underlying factors of flood risk in both scenarios. This discussion section is organized into five parts. First, it discusses the nuanced differences between top underlying factors in dual flood damage scenarios. Second, it highlights the major flood-risk cities along the USGAC. Third, it presents a comparative analysis of two major flood-risk cities located on two different coasts. Fourth, it offers some policy recommendations on mitigating flood risk in major flood risk cities. Last, it discusses the limitations of this study.

Underlying FRFs

Under both scenarios, the most influential variables include elevation, drainage density, population density, precipitation, building height, and distance from rivers and the coast. For the GFD scenario, low elevation is the most critical factor, whereas high drainage density plays the primary role for EFD (Fig. 5). Previous research (*9*, *32*–*36*) consistently found that low elevation (as water naturally flows from higher to lower altitude regions), high precipitation (which can overwhelm drainage systems with large volume of water), and proximity to water bodies (which increases exposure to

riverine flooding or storm surge) played major roles in flood risk. These findings are extensively documented around the world, such as in Adana Province, Turkey (*32*); Harris County, Texas (*9*); West Bengal, India (*33*); Slovakia (*33*); Bangladesh (*34*); and Kunming, China (*35*). This study further reveals that, under the EFD scenario, high drainage density is the dominant factor. The occurrence of EFD is influenced by several hydrodynamic factors such as high discharge velocity, rapid surface runoff, and flood depth. Areas with high drainage density tend to experience faster surface runoff and higher peak discharge because high drainage density facilitates rapid water flow to channels after a rainfall (*36*). Consequently, the probability of EFD increases within highly developed urban areas located in dense natural drainage networks. Although high natural drainage networks can generally mitigate flooding by efficiently directing water toward rivers and the ocean after heavy rainfall events, this protective effect is often compromised in urbanized landscapes. The construction of impervious infrastructures, such as roads, parking lots, and buildings, can disrupt natural drainage systems by filling wetlands or obstructing flow paths. This forces floodwaters to interact with built structures, reduces infiltration, accelerates runoff, and produces larger flood volumes with shorter times to peak (*37*). As a result, such conditions exacerbate the impact on human infrastructure, leading to extreme damage and substantial economic losses. Moreover, flood risk is particularly high in regions with dense drainage networks that are also densely populated with low-quality buildings, such as single-story wooden structures (*38*).

Major flood-risk cities

This study identifies high flood risk zones along the USGAC and reveals that, although a small portion of the area is classified at high flood risk, a large portion of the population lives there. These findings indicate that flood risk is particularly high in densely populated cities. A recent study (*4*) projected that, by 2050, major cities along the USGAC will face 1301 to 1777 km^2 of additional high-tide flooding, affecting millions of people and properties, and placing $28 billion to $85 billion in property value at risk. Another study (*31*) highlighted that 60% of the census blocks are experiencing high to very high flood risk adjacent to of the Gulf Coast. These findings altogether highlight the urgent need to strengthen flood protection measures in major flood-prone cities across the USGAC. Some major cities such as New Orleans, New York, Houston, and Mobile are at high risk under both scenarios, demanding prioritized attention from policy-makers. By contrast, some cities such as Charleston, Norfolk, Jacksonville, and Miami are at high risk under the GFD scenario, but their risk levels decrease notably in the EFD case.

A tale of two cities

This study identifies two major flood-risk cities along the two coasts: New York (NYC), which has the largest exposed populations and buildings, and New Orleans (NOLA), which has the highest percentage of exposed population and building. Despite their distinct geographic locations, climates, topographies, and social-demographic compositions, both cities share a grim reality: a high risk of flooding.

NYC is among the top 10 cities worldwide in terms of assets exposed to coastal flooding, with nearly 15% of its area in the 100-year flood zone (*39*). The flood condition has been intensified by both natural characteristics and anthropogenic factors (*40*). Tropical cyclones bring a combination of heavy rainfall and storm surge, overwhelming the city's largely paved drainage systems. This increased hurricane-induced flood risk leads to severe impacts on both human communities and ecological systems (*6*). Two recent hurricanes, Hurricane Sandy (2012) and Hurricane Ida (2021), caused severe casualties and infrastructure damages (*41*). This is largely due to dense urban development replacing natural drainage with impervious surfaces, which increases surface runoff, reduces infiltration, and overwhelms sewer systems, leading to frequent pluvial flooding. Meanwhile, gradual sea level rise impedes the drainage of tidal rivers and streams, increasing fluvial flood risk. In addition, historical development on landfill over tidal marshes and nearshore zones, along with extensive dredging in areas like Jamaica Bay, has made the city highly vulnerable to coastal flooding (*11*). Land subsidence at a rate of 1 to 2 mm/year, caused by excessive groundwater pumping and dredging, exacerbates overall flood risk (*40*). Together, these factors make New York City at high risk of multiple forms of flooding.

In addition to its physical and infrastructure characteristics, NYC's highly dense population (~8.8 millions) with high social vulnerability amplifies the potential impacts of flooding. A substantial proportion of residents are identified as socially vulnerable groups, including low-income households, economically disadvantaged minority communities, immigrants, and elderly individuals, all of whom face disproportionate flood-related risks (*39*, *41*).

Greater New Orleans (NOLA) is bordered by the Mississippi River, Lake Pontchartrain, and the Gulf of America, surrounded by extensive wetlands and natural drainage networks (*42*). Situated in a bowl-shaped basin largely below sea level, the city experiences mean and maximum subsidence rates of ~6.4 and ~33 mm/year (*43*). It experiences heavy rainfall due to climate change with an average of 1623 mm (64 inches) of annual precipitation and high storm surge (*44*). Its drainage entirely relies on pumps to evacuate water because gravity drainage is limited by its bowl-shaped low elevation (*42*, *45*). These physical conditions of this city make it highly susceptible to flooding.

NOLA has recently experienced multiple high-impact floods, with Hurricane Katrina (2005) being the most notable, which drew widespread attention for the severe damages and losses (*46*). Its history with social inequality and racial injustice exacerbated the impact of Hurricane Katrina and slowed the recovery. Vulnerable groups such as people living in poverty and those with less education and low housing quality were heavily affected (*44*, *47*). For instance, the highest damage was observed in places where most of the residential buildings were built on wood materials with less resistance to flooding (*38*). Socially disadvantaged groups inhabit the city's low-lying areas, where their vulnerability exacerbates the impacts of flooding (*48*). According to the First Street Foundation (*49*), 30 years from now, a 100-year flood event is projected to affect 148,952 properties that represent 99.6% of all properties in NOLA. These findings closely align with our results, showing that nearly all residents (~99%) in New Orleans are at high risk of flooding under both scenarios (GFD and EFD).

To conclude, NYC's flood risk is shaped by multiple interacting factors. Dense urbanization limits the availability of permeable surfaces, which reduces natural water absorption and increases surface runoff during heavy rainfall. Aging and overburdened infrastructure further exacerbates the problem as drainage and sewage systems struggle to cope with extreme precipitation events that are becoming more frequent under climate change. Land subsidence caused by dredging and groundwater pumping contributes to a gradual lowering of land elevation, exacerbating the city's long-term vulnerability to sea level rise. By contrast, NOLA faces an even more

acute flood risk due to its unique geographic and environmental conditions. The city's low-lying and bowl-shaped topography places much of its land below sea level, exposing it to flooding from storm surge, river overflow, and heavy rainfall. To make things worse, the city is surrounded by dense water bodies and wetlands networks, while offering some natural protection, can be overwhelmed during extreme events. NOLA's heavy reliance on engineered defense systems such as pumps and levees add one more layer of vulnerability as a weak link in the entire system can lead to catastrophic flooding. Compounding these risks, the city experience one of the highest rates of land subsidence in the US, further lowering elevation and intensifying the impacts of sea level rise. Together, the combination of urbanization, infrastructure pressure, and land subsidence in NYC, alongside the extreme geographic and social structural profiles of NOLA, make both cities among the most at risk of flooding in general and severe flooding in particular in the US.

Policy recommendations

To effectively mitigate flood risk in densely populated coastal cities like New York and New Orleans, an integrated policy approach is required that actively engages local stakeholders. Such policies should restrict further urban development in high-risk zones while promoting the systematic incorporation of nature-based solutions including green and blue infrastructure alongside traditional gray infrastructure within flood risk mitigation planning (*39*, *50*).

Green infrastructure can play a vital role in reducing surface flooding by replacing impervious surfaces with permeable alternatives such as grasslands, rain gardens, bioswales, and lawns. For example, parking lots are typically constructed using impervious concrete, which can be replaced with permeable concrete or grass tiles, allowing rainwater to infiltrate directly into the soil. In addition, vegetated infiltration strips and bioswales can be implemented along the roadway or sidewalk to further slow surface runoff and reduce peak flows, whereas street tree plantation can further enhance soil infiltration through their root systems and increase evapotranspiration by intercepting rainfall through their canopies. Collectively, these green infrastructure practices can substantially reduce surface runoff before it overwhelms urban drainage systems.

Blue infrastructure, including natural wetlands, river floodplains, and estuaries, should be restored and strategically connected to urban drainage and sewerage networks. Rain-fed peatlands, bogs, swamp forest, and marshland can function as natural sponges, absorbing and gradually releasing rainfall, whereas river floodplains, fens, and wet meadows can act as large water storage of surface water runoff from surrounding the city. Restoring wetlands and river floodplains and linking them with urban drainage systems can facilitate faster discharge of floodwaters from cities following extreme events. Large coastal cities surrounded by extensive waterbodies, river networks, and wetlands, such as New Orleans and New York, can particularly benefit from these blue infrastructure practices. In addition, temporary water storage systems can help mitigate sewage overflows during extreme precipitation events.

Gray infrastructure such as levees, dikes, floodgates, embankments, and seawalls remains essential but should be complemented rather than replace nature-based solutions. In addition, efficiently designed pumping and sewer systems need to be further enhanced to ensure the rapid evacuation of floodwater. In parallel, flood communication systems, including early warning and public alert tools, should be strengthened and modernized. Reducing false alarms must be prioritized to improve public trust, response effectiveness, and overall risk perception.

In particular, in New Orleans, where unique geography and severe land subsidence amplify long-term risks, managed retreat should be on the policy agenda for the riskiest areas to minimize future exposure. Last, building resilient communities through sustainable public education and targeted urban planning is vital for strengthening adaptive capacity and reducing the impacts of increasing flood risk.

Limitations

We need to acknowledge several limitations. First, the ML models rely on historical flood damage data as the target variable, which may not fully capture future dynamics under climate change. In addition, incorporating more flood damage locations from a larger number of flood events spanning broader spatial and temporal extents would further improve ML model training and robustness. Second, although ML models have achieved strong predictive performances, this data-driven approach, without considering the underlying complex physical process, is highly subject to the quality of data and selection of risk factors. Third, the analysis is made on two scenarios (GFD and EFD), which does not account for a spectrum of scenarios such as the cascading impacts of compound flooding. Overall, the framework's scalability beyond the USGAC requires careful adaptation to local contexts.

Future research should incorporate additional flood damage locations from a larger number of events across broader spatial and temporal scales. Integrating climate projections can help capture the future dynamics of flood risk, whereas including compound flood events can provide a more comprehensive assessment. In addition, complementing data-driven ML models with physics-based models can enhance the robustness and reliability of predictions.

MATERIALS AND METHODS

This study primarily required two key elements: flood damage data and FRFs, both of which were integrated into the ML models (Fig. 2). Here, we used flood damage data as target variables and FRFs as predictor variables. The methodological process of this study is briefly described below.

Flood damage data

Flood damage refers to the destruction and physical impacts to human structures caused by floodwater inundation. It can be classified as direct (from physical contact with floodwater) and indirect (secondary impacts occurring across time or space) damage (*8*). This study used direct flood damages to human structure/properties from the Federal Emergency Management Agency (FEMA) website (https://disasters-geoplatform.hub.arcgis.com/pages/historical-damage-assessment-database). However, this website contains damaged data that occurred due to flooding, hurricane winds, and multievent impacts. For this study, we initially filtered out all structural damage points associated with hurricane winds and multievent events within the study area. Then, we selected a total of 52,710 flood damage locations, including all levels of damages, i.e., affected, minor, major, and destroyed, as the target variable for the GFD scenario, whereas we used a subset of 19,272 destroyed locations as the target variables for the EFD scenario (Fig. 6A). Here, we classified affected, minor, and major damage to human structures based on indicators such as missing floor segments,

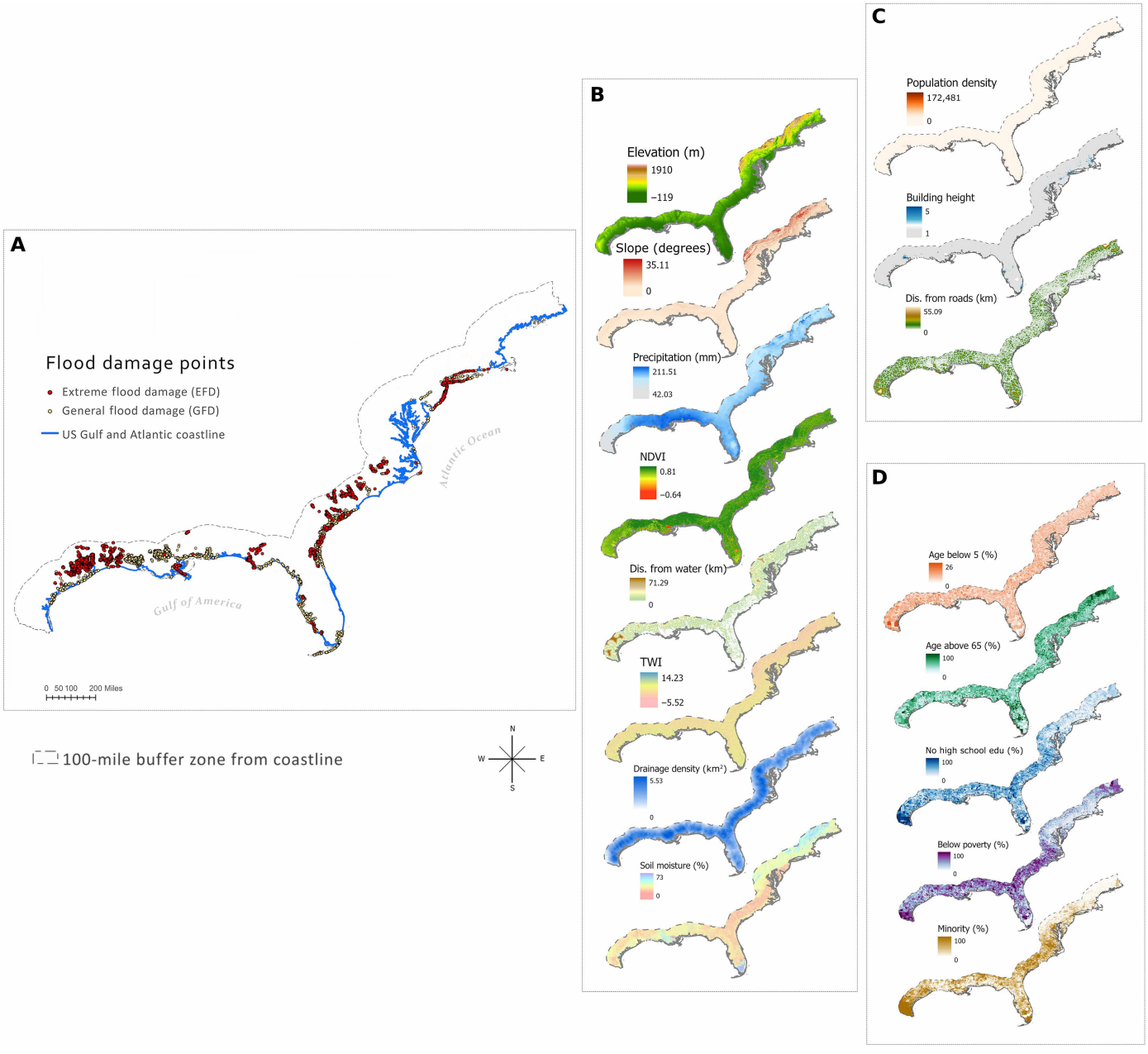

Fig. 6. Flood damage data and FRFs used in this study. (**A**) Locations of flood damage along the USGAC. Yellow dots represent the locations of the GFD location, whereas red dots represent the locations of the EFD location. (**B**) FRFs from hazard. (**C**) FRFs from exposure. (**D**) FRFs from vulnerability.

failure of structural elements, and other visible damage, whereas we classified destroyed structures as fully collapsed based on post-event image analysis or FEMA flood depth grid modeling.

These flood damage locations were associated with multiple recent major flood events including 2012 Hurricane Isaac, 2012 Hurricane Sandy, 2016 Hurricane Hermine, 2016 Hurricane Matthew, 2016 Louisiana Flood, 2017 Hurricane Harvey, 2017 Hurricane Irma, and 2017 Hurricane Nate. We labeled flood damage points as 1. We randomly generated non–damage points throughout the study area and labeled them as 0. We combined these two sets of points into a single sample set for each scenario. We used these sample points locations to extract their corresponding values for all the predictors variables (FRFs). Then, we used 70% of the sample data to train the ML models and 30% for testing (Fig. 2).

Flood risk factors

A variety of factors, including topography, precipitation pattern, geological features, vegetation cover, and anthropogenic features, play a critical role in shaping flood dynamics, either through direct or indirect influence. They are known as FRFs (*25*). On the basis of extensive literature review, we selected a total of 16 FRFs, including eight hazard-related factors (Fig. 6B), three exposure-related factors

(Fig. 6C), and five vulnerability-related factors (Fig. 6D). We collected these FRFs from multiple reliable sources and processed using platforms including Google Earth Engine, Python, and ArcGIS Pro (Table 2). To maintain consistency in scale and spatial extent, we resampled all FRFs to a 250-m resolution and projected them to the World Geodetic System 1984 coordinate system. We also conducted a multicollinearity analysis to assess correlations among the variables. On the basis of a threshold of ±0.8, we identified no severe correlations among FRFs.

Performance evaluation and uncertainty test of ML models

We adopted three supervised ML models: SVM, RF, and MLP, which represent the linear, tree-based, and neural network algorithm families, respectively, in this study. To identify the best-performing ML model, we first applied the ROC-AUC, a widely accepted metric for assessing predictive accuracy that measures the AUC formed by plotting the true-positive rate against the false-positive rate (*51*), to the testing set to compare model performance in flood risk prediction. Following that, we conducted a comprehensive evaluation using multiple performance metrics, including accuracy, precision, recall, F1 score, kappa score, and Jaccard score, to ensure rigorous model validation. We then selected the best-performing ML model (RF model) based on the highest average score across all evaluation metrics, including ROC-AUC (Fig. 7).

The uncertainty test is crucial but often overlooked in flood modeling. Because it directly influences the reliability and accuracy of results and decision-making, a robust framework is essential to assess and reduce uncertainty in flood research (*52*). We used the Shannon entropy algorithm to assess the uncertainty of the best-performing ML model (RF model). This algorithm has several applications across scientific fields, including the measurement of uncertainty or randomness of probability distribution (*53*). On the basis of the analysis,

Table 2. List of FRFs from hazard, exposure, and vulnerability with descriptions and data sources.

	FRFs	Descriptions	Source	Spatial resolution	Temporal resolution	Band
Hazard	Elevation (DEM)	Elevation substantially influences surface runoff and flow toward low altitude regions during flood.	NASA/USGS/ SRTM V003	30 m	2000 (last updated in 2015)	elevation
	Slope	Slope influences the speed and direction of floodwater to accumulate.	DEM	30 m	–	–
	Precipitation	Precipitation is the primary source of floodwater, which led rivers to overflow and inundate nearby floodplains.	PRISM/ OREGON STATE	928 m	1991–2020	ppt
	NDVI	Vegetation covers hinder surface runoff and promotes infiltration and percolation processes.	Landsat 8	30 m	2010–2022	B4, B5
	Distance from water	Distance from waterbodies affects flood extent and severity as the regions close to river and coast are more prone to inundation.	USA Detailed Water Bodies	Polyline	2023	–
	TWI	TWI refers to the spatial distribution of wetness across a region that affects surface flow.	DEM	30 m	–	–
	Drainage density	Drainage density, the ratio of the total channel length to basin area, influences surface runoff and overall water discharge.	DEM	30 m	–	–
	Soil moisture	Soil moisture, the percentage of water in the soil that affects both percolation and surface runoff.	Open Land Map	250 m	2019	b0 (at 0-cm depth)
Exposure	Population density	Population density refers to the number of populations living within a certain area.	CDC/ATSDR	Census tracts	2020	–
	Building height	Building heights refers to the average height of buildings in block groups.	USGS	Block groups	2016	–
	Distance from roads	Dense roads make an impermeable surface that prevents water percolation and speeds up surface runoff.	US Census Bureau/ TIGER	Polyline	2023	–
Vulnerability	Age below 5	The percentage of the population aged under 5 years old.	US Census Bureau	Census tracts	2020	–
	Age above 65	The percentage of the population aged above 65 years old.	CDC/ATSDR	Census tracts	2020	–
	No high school diploma	The percentage of population with no high school diploma (age 25+).	CDC/ATSDR	Census tracts	2020	–
	Below poverty	The percentage of population below 150% poverty.	CDC/ATSDR	Census tracts	2020	–
	Minorities	The percentage of minorities (Hispanic, African American, American Indian, Alaska Native, Native Hawaiian, and so on).	CDC/ATSDR	Census tracts	2020	–

only 11.7% of the test samples showed high entropy (>0.5) under the GFD scenario and 9% under the EFD scenario (Fig. 8, A and B). The uncertainty maps indicate that most regions in the USGAC had low entropy (<0.2) in both cases (Fig. 8, C and D), which demonstrate the reliability of the RF model. We conducted the entire process in Python in Jupyter Notebook.

Dual-scenario flood risk mapping

We selected the best-performing RF model to predict dual-scenario flood risk probabilities along the USGAC. We conducted the entire workflow was conducted in Python using a Jupyter Notebook environment. We generated the predicted values, referred to as the flood risk index (FRI), for both GFD and EFD scenarios and exported in

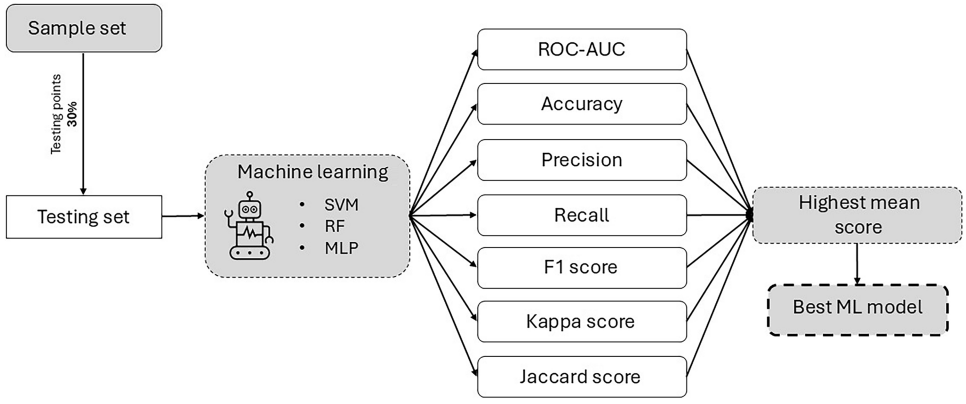

Fig. 7. Flowchart of the process of selecting the best ML model.

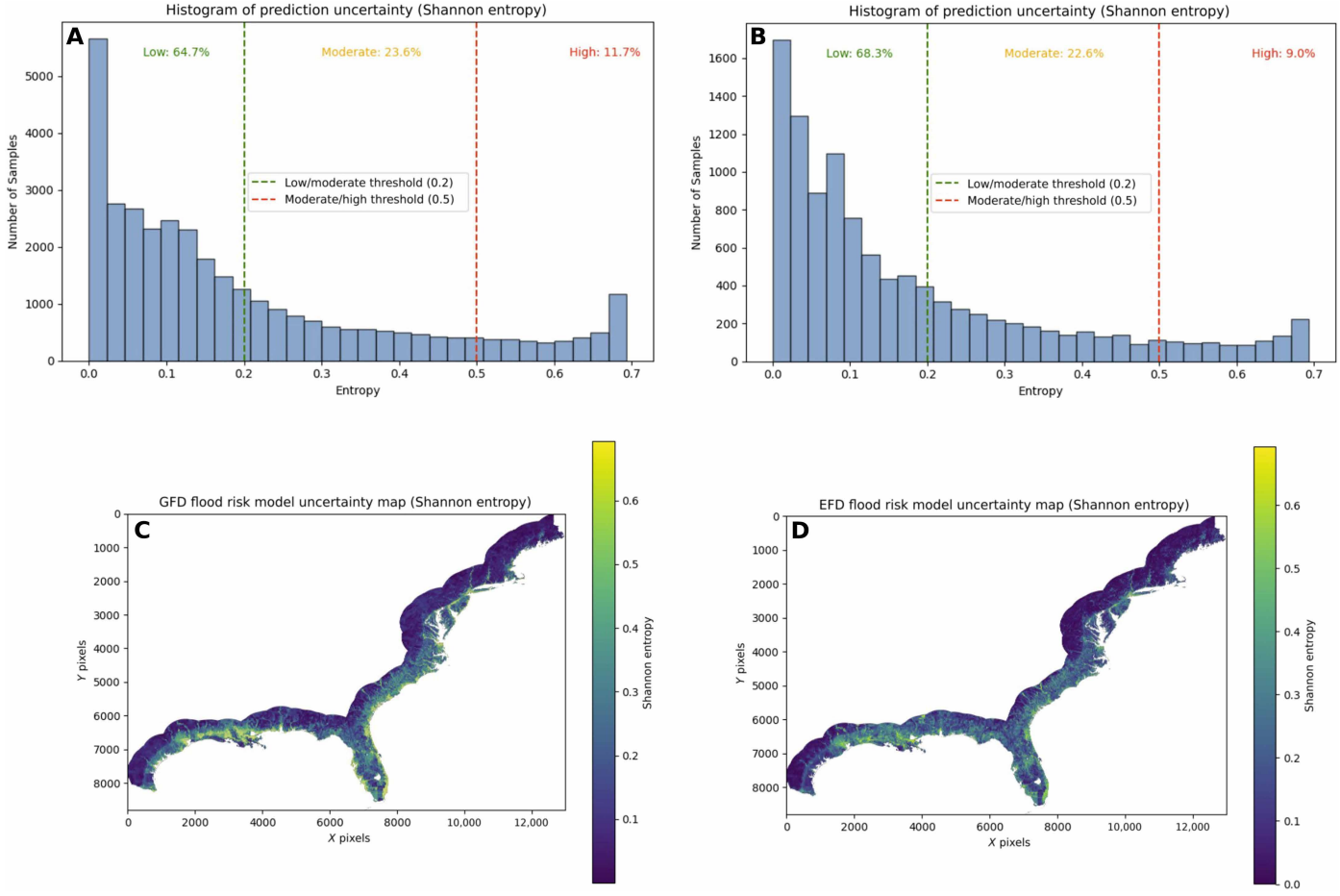

Fig. 8. Uncertainty test using Shannon entropy. (**A**) Histogram of Shannon entropy values for GFD test samples. (**B**) Histogram of Shannon entropy values for EFD test samples. (**C**) Uncertainty map based on Shannon entropy for GFD. (**D**) Uncertainty map based on Shannon entropy for EFD.

GeoTIFF format. The FRI values range from 0 to 1, where values close to 0 represent low risk and values close to 1 indicate high risk. We then classified these FRI values classified into five different risk categories—very high, high, moderate, low, and very low—using natural break classification methods. Last, we prepared flood risk maps for both scenarios and tabulated results.

Unveiling flood-prone coastal cities by estimating potential exposure

To identify flood-prone cities along the USGAC, we initially selected eight cities based on hotspots of very high and high-risk zones under both scenarios. Then, we used city boundary shapefiles to clip the raster files, merged the very high and high-risk zones, and converted it into vector format (polygon file). Using this merged polygon file, we estimated population and building footprints within these high-risk areas applying the "Select by Location" tool in ArcGIS Pro. To estimate the number of exposed populations, we used 2020 US Census population data and used Microsoft's building footprint dataset to estimate the number of exposed buildings. On the basis of both the absolute exposed population and the percentage of population at high flood risk, we selected two cities for further discussion.

Underlying factor analysis

We identified the major underlying factors under both scenarios using SHAP tools. The SHAP, a powerful XAI tool (*54*), not only ranks the contributions of FRFs but also illustrates how much each factor influences the model's predictions. SHAP summary plots compile SHAP values from all instances to show how important each feature is for the models' training (*55*). We generated the SHAP summary plots for both scenarios using Python in Jupyter Notebook.

REFERENCES

1. K. T. Antwi-Agyakwa, M. K. Afenyo, D. B. Angnuureng, Know to predict, forecast to warn: A review of flood risk prediction tools. *Water* **15**, 427 (2023).
2. J. Rentschler, M. Salhab, B. A. Jafino, Flood exposure and poverty in 188 countries. *Nat. Commun.* **13**, 3527 (2022).
3. E. L. Collins, G. M. Sanchez, A. Terando, C. C. Stillwell, H. Mitasova, A. Sebastian, R. K. Meentemeyer, Predicting flood damage probability across the conterminous United States. *Environ. Res. Lett.* **17**, 034006 (2022).
4. L. O. Ohenhen, M. Shirzaei, C. Ojha, S. F. Sherpa, R. J. Nicholls, Disappearing cities on US coasts. *Nature* **627**, 108–115 (2024).
5. R. Marsooli, N. Lin, K. Emanuel, K. Feng, Climate change exacerbates hurricane flood hazards along US Atlantic and Gulf Coasts in spatially varying patterns. *Nat. Commun.* **10**, 3785 (2019).
6. M. Sajjad, N. Lin, J. C. L. Chan, Spatial heterogeneities of current and future hurricane flood risk along the U.S. Atlantic and Gulf coasts. *Sci. Total Environ.* **713**, 136704 (2020).
7. C. Li, N. Sun, Y. Lu, B. Guo, Y. Wang, X. Sun, Y. Yao, Review on urban flood risk assessment. *Sustainability* **15**, 765 (2023).
8. B. Merz, H. Kreibich, R. Schwarze, A. Thieken, Review article "Assessment of economic flood damage". *Nat. Hazards Earth Syst. Sci.* **10**, 1697–1724 (2010).
9. H. Dey, W. Shao, M. M. Haque, M. VanDyke, Enhancing flood risk analysis in harris county: Integrating flood susceptibility and social vulnerability mapping. *J. Geovisualization Spat. Anal.* **8**, 19 (2024).
10. M. Eini, H. S. Kaboli, M. Rashidian, H. Hedayat, Hazard and vulnerability in urban flood risk mapping: Machine learning techniques and considering the role of urban districts. *Int. J. Disaster Risk Reduct.* **50**, 101687 (2020).
11. B. Rosenzweig, F. A. Montalto, P. Orton, J. Kaatz, N. Maher, J. Kleyman, Z. Chen, E. Sanderson, N. Adhikari, T. McPhearson, P. Herreros-Cantis, NPCC4: Climate change and New York City's flood risk. *Ann. N. Y. Acad. Sci.* **1539**, 127–184 (2024).
12. Y. Wang, Q. Zhang, K. Lin, Z. Liu, Y.-s. Liang, Y. Liu, C. Li, A novel framework for urban flood risk assessment: Multiple perspectives and causal analysis. *Water Res.* **256**, 121591 (2024).
13. IPCC, "Climate Change 2014: Impacts, Adaptation, and Vulnerability. Part A: Global and Sectoral Aspects. Contribution of Working Group II to the Fifth Assessment Report of the Intergovernmental Panel on Climate Change," C. B. Field, V. R. Barros, D. J. Dokken, K. J. Mach, M. D. Mastrandrea, T. E. Bilir, M. Chatterjee, K. L. Ebi, Y. O. Estrada, R. C. Genova, B. Girma, E. S. Kissel, A. N. Levy, S. MacCracken, P. R. Mastrandrea, L. L. White, Eds. (Cambridge Univ. Press, 2014), 1132 pp.
14. H. Dey, M. M. Haque, W. Shao, M. VanDyke, F. Hao, Simulating flood risk in Tampa Bay using a machine learning driven approach. *NPJ Nat. Hazards* **1**, 40 (2024).
15. E. E. Koks, B. Jongman, T. G. Husby, W. J. W. Botzen, Combining hazard, exposure and social vulnerability to provide lessons for flood risk management. *Environ. Sci. Policy* **47**, 42–52 (2015).
16. B. Choubin, E. Moradi, M. Golshan, J. Adamowski, F. Sajedi-Hosseini, A. Mosavi, An ensemble prediction of flood susceptibility using multivariate discriminant analysis, classification and regression trees, and support vector machines. *Sci. Total Environ.* **651**, 2087–2096 (2019).
17. H. Dey, W. Shao, H. Moradkhani, B. D. Keim, B. G. Peter, Urban flood susceptibility mapping using frequency ratio and multiple decision tree-based machine learning models. *Nat. Hazards* **120**, 10365–10393 (2024).
18. H. Shahabi, A. Shirzadi, K. Ghaderi, E. Omidvar, N. Al-Ansari, J. J. Clague, M. Geertsema, K. Khosravi, A. Amini, S. Bahrami, O. Rahmati, K. Habibi, A. Mohammadi, H. Nguyen, A. M. Melesse, B. B. Ahmad, A. Ahmad, Flood detection and susceptibility mapping using sentinel-1 remote sensing data and a machine learning approach: Hybrid intelligence of bagging ensemble based on K-nearest neighbor classifier. *Remote Sens.* **12**, 266 (2020).
19. A. Mosavi, P. Ozturk, K.-w. Chau, Flood prediction using machine learning models: Literature review. *Water* **10**, 1536 (2018).
20. N. S. Romali, S. Sulong, A. Kawasaki, A systematic review of flood damage assessment: Insight for the data-scarce regions. *Water Resour. Manag.* **39**, 4707–4734 (2025).
21. B. Pradhan, S. Lee, A. Dikshit, H. Kim, Spatial flood susceptibility mapping using an explainable artificial intelligence (XAI) model. *Geosci. Front.* **14**, 101625 (2023).
22. M. S. Tehrany, M.-J. Lee, B. Pradhan, M. N. Jebur, S. Lee, Flood susceptibility mapping using integrated bivariate and multivariate statistical models. *Environ. Earth Sci.* **72**, 4001–4015 (2014).
23. M. Sahana, S. Rehman, H. Sajjad, H. Hong, Exploring effectiveness of frequency ratio and support vector machine models in storm surge flood susceptibility assessment: A study of Sundarban Biosphere Reserve, India. *Catena* **189**, 104450 (2020).
24. K. Khosravi, B. T. Pham, K. Chapi, A. Shirzadi, H. Shahabi, I. Revhaug, I. Prakash, D. Tien Bui, A comparative assessment of decision trees algorithms for flash flood susceptibility modeling at Haraz watershed, Northern Iran. *Sci. Total Environ.* **627**, 744–755 (2018).
25. M. B. Kia, S. Pirasteh, B. Pradhan, A. R. Mahmud, W. N. A. Sulaiman, A. Moradi, An artificial neural network model for flood simulation using GIS: Johor River Basin, Malaysia. *Environ. Earth Sci.* **67**, 251–264 (2011).
26. Y. Wang, Z. Fang, H. Hong, L. Peng, Flood susceptibility mapping using convolutional neural network frameworks. *J. Hydrol.* **582**, 124482 (2020).
27. Y. Qin, X. Yin, Y. Li, Q. Xu, L. Zhang, P. Mao, X. Jiang, High-precision flood mapping from sentinel-1 dual-polarization SAR data. *IEEE Trans. Geosci. Remote Sens.* **63**, 4204315 (2025).
28. F. Yarveysi, A. Alipour, H. Moftakhari, K. Jafarzadegan, H. Moradkhani, Block-level vulnerability assessment reveals disproportionate impacts of natural hazards across the conterminous United States. *Nat. Commun.* **14**, 4222 (2023).
29. N. S. Grigg, Comprehensive flood risk assessment: State of the practice. *Hydrology* **10**, 46 (2023).
30. S. M. H. S. Rezvani, A. Gonçalves, M. J. F. Silva, N. M. de Almeida, Smart hotspot detection using geospatial artificial intelligence: A machine learning approach to reduce flood risk. *Sustain. Cities Soc.* **115**, 105873 (2024).
31. F. Yarveysi, K. Jafarzadegan, S. S. Tripathy, H. Moftakhari, H. Moradkhani, A data-driven framework for an efficient block-level coastal flood risk assessment. *Int. J. Disaster Risk Reduct.* **122**, 105478 (2025).
32. H. E. Aydin, M. C. Iban, Predicting and analyzing flood susceptibility using boosting-based ensemble machine learning algorithms with SHapley Additive exPlanations. *Nat. Hazards* **116**, 2957–2991 (2023).
33. M. Vojtek, J. Vojteková, Flood susceptibility mapping on a national scale in Slovakia using the analytical hierarchy process. *Water* **11**, 364 (2019).
34. P. Debnath, A. Biswas, G. Jeong, Review of the use of the analytical hierarchy process for flood risk assessment in Bangladesh. *Nat. Hazards* **121**, 19443–19472 (2025).
35. H. Ren, B. Pang, P. Bai, G. Zhao, S. Liu, Y. Liu, M. Li, Flood susceptibility assessment with random sampling strategy in ensemble learning (RF and XGBoost). *Remote Sens.* **16**, 320 (2024).
36. F. L. Ogden, N. Raj Pradhan, C. W. Downer, J. A. Zahner, Relative importance of impervious area, drainage density, width function, and subsurface storm drainage on flood runoff from an urbanized catchment. *Water Resour. Res.* **47**, W12503 (2011).
37. K. Jafarzadegan, H. Moradkhani, F. Pappenberger, H. Moftakhari, P. Bates, P. Abbaszadeh, R. Marsooli, C. Ferreira, H. L. Cloke, F. Ogden, Q. Duan, Recent advances and new frontiers in Riverine and Coastal flood modeling. *Rev. Geophys.* **61**, e2022RG000788 (2023).
38. A. K. Pistrika, S. N. Jonkman, Damage to residential buildings due to flooding of New Orleans after hurricane Katrina. *Nat. Hazards* **54**, 413–434 (2010).

39. Y. Depietri,T. McPhearson, "Integrating the grey, green, and blue in cities: Nature-based solutions for climate change adaptation and risk reduction" in *Nature-Based Solutions to Climate Change Adaptation in Urban Areas* (Springer, 2017), pp. 91–109.
40. T. Parsons, P. C. Wu, M. Wei, S. D'Hondt, The weight of New York City: Possible contributions to subsidence from anthropogenic sources. *Earths Future* **11**, e2022EF003465 (2023).
41. G. Anand, P. J. Marcotullio, Spatial disparities in flood vulnerability in New York City. *J. Hosp. Manag. Health Policy* **8**, 4 (2024).
42. F. Boogaard, D. Rooze, R. Stuurman, The long-term hydraulic efficiency of green infrastructure under sea level: Performance of raingardens, swales and permeable pavement in New Orleans. *Land* **12**, 171 (2023).
43. T. H. Dixon, F. Amelung, A. Ferretti, F. Novali, F. Rocca, R. Dokka, G. Sella, S.-W. Kim, S. Wdowinski, D. Whitman, Subsidence and flooding in New Orleans. *Nature* **441**, 587–588 (2006).
44. H. Cai, N. Lam, L. Zou, Y. Qiang, K. Li, Assessing community resilience to coastal hazards in the Lower Mississippi river basin. *Water* **8**, 46 (2016).
45. P. B. Kane, N. Tebyanian, D. Gilles, B. McMann, J. R. Fischbach, Key drivers of vulnerability to rainfall flooding in New Orleans. *Front. Clim.* **6**, 1303951 (2024).
46. B. D. M. Keim, *Hurricanes of the Gulf of Mexico* (LSU Press, 2009).
47. C. Finch, C. T. Emrich, S. L. Cutter, Disaster disparities and differential recovery in New Orleans. *Popul. Environ.* **31**, 179–202 (2010).
48. S. Garcia-Rosabel, D. Idowu, W. Zhou, At the intersection of flood risk and social vulnerability: A case study of New Orleans, Louisiana, USA. *GeoHazards* **5**, 866–885 (2024).
49. First Street Foundation, "New Orleans, LA flood risk" (2025).
50. J. Griffiths, K. E. Borne, A. Semadeni-Davies, C. C. Tanner, Selection, planning, and modelling of nature-based solutions for flood mitigation. *Water* **16**, 2802 (2024).
51. D. Sarkar, P. Mondal, Flood vulnerability mapping using frequency ratio (FR) model: A case study on Kulik river basin, Indo-Bangladesh Barind region. *Appl. Water Sci.* **10**, 17 (2019).
52. K. Xu, C. Wang, L. Bin, Compound flood models in coastal areas: A review of methods and uncertainty analysis. *Nat. Hazards* **116**, 469–496 (2023).
53. N. Ivan Ulloa, S.-H. Chiang, S.-H. Yun, Flood proxy mapping with normalized difference sigma-naught index and Shannon's entropy. *Remote Sens.* **12**, 1384 (2020).
54. S. M. L. Lundberg, S.-I. Lee, "A unified approach to interpreting model predictions," in *Proceedings of the 31st International Conference on Neural Information Processing Systems* (Curran Associates Inc., 2017).
55. M. Waleed, M. Sajjad, High-resolution flood susceptibility mapping and exposure assessment in Pakistan: An integrated artificial intelligence, machine learning and geospatial framework. *Int. J. Disaster Risk Reduct.* **121**, 105442 (2025).

Acknowledgments

Funding: Funding for this project was provided by the National Oceanic and Atmospheric Administration (NOAA), awarded to the Cooperative Institute for Research on Hydrology (CIROH) through the NOAA Cooperative Agreement with The University of Alabama (NA22NWS4320003). W.S. received this grant. **Author contributions:** Conceptualization: H.D. and W.S. Methodology: H.D. Software: H.D. Validation: H.D. Formal analysis: H.D. Investigation: W.S. Resources: W.S. Data curation: H.D. Visualization: H.D. Supervision: W.S. Project administration: W.S. Funding acquisition: W.S. Writing—original draft: H.D. and W.S. Writing—review and editing: H.D. and W.S. **Competing interests:** The authors declare that they have no competing interests. **Data, code, and materials availability:** All data and code needed to evaluate and reproduce the results in the paper are present in the paper and a Dryad repository (https://doi.org/10.5061/dryad.bzkh189q7). This study did not generate new materials.

Submitted 18 September 2025
Accepted 20 March 2026
Published 22 April 2026
10.1126/sciadv.aec2079

ScienceAdvances

A tale of two coasts: Unveiling US Gulf and Atlantic coastal cities at high flood risk

Hemal Dey and Wanyun Shao

Sci. Adv. **12** (17), eaec2079. DOI: 10.1126/sciadv.aec2079